ChemPubSoc Europe

DOI: 10.1002/cctc.201200580

Mechanistic Studies on Chabazite-Type Methanol-to-Olefin Catalysts: Insights from Time-Resolved UV/Vis Microspectroscopy Combined with Theoretical Simulations

Veronique Van Speybroeck,*[a] Karen Hemelsoet,[a] Kristof De Wispelaere,[a] Qingyun Qian,[b] Jeroen Van der Mynsbrugge,[a] Bart De Sterck,[a] Bert M. Weckhuysen,*[b] and Michel Waroquier[a]

The formation and nature of active sites for methanol conversion over solid acid catalyst materials are studied by using a unique combined spectroscopic and theoretical approach. A working catalyst for the methanol-to-olefin conversion has a hybrid organic–inorganic nature in which a cocatalytic organic species is trapped in zeolite pores. As a case study, microporous materials with the chabazite topology, namely, H-SAPO-34 and H-SSZ-13, are considered with trapped (poly)aromatic species. First-principle rate calculations on methylation reactions and in situ UV/Vis spectroscopy measurements are performed. The theoretical results show that the structure of the organic compound and zeolite composition determine the methylation rates: 1) the rate increases by 6 orders of magnitude if more methyl groups are added on benzenic species, 2) transition state selectivity occurs for organic species with more than one aromatic core and bearing more than three methyl groups, 3) methylation rates for H-SSZ-13 are approximately 3 orders of magnitude higher than on H-SAPO-34 owing to its higher acidity. The formation of (poly)aromatic cationic compounds can be followed by using in situ UV/Vis spectroscopy because these species yield characteristic absorption bands in the visible region of the spectrum. We have monitored the growth of characteristic peaks and derived activation energies of formation for various sets of (poly)aromatic compounds trapped in the zeolite host. The formation–activation barriers deduced by using UV/Vis microspectroscopy correlate well with the activation energies for the methylation of the benzenic species and the lower methylated naphthalenic species. This study shows that a fundamental insight at the molecular level can be obtained by using a combined in situ spectroscopic and theoretical approach for a complex catalyst of industrial relevance.

Introduction

Light olefins are crucial compounds in today's petrochemical industry and are traditionally obtained through the refinement of crude oil. In view of the waning oil reserves, the development of new technologies for the production of chemicals and transportation fuels based on alternative natural sources is very topical.[1] Of these processes, the zeolite-catalyzed methanol-to-hydrocarbon (MTH) technology is one of the most promising and several MTH processes have currently been commercialized.[2,3] The ability of acid zeolites to convert methanol to hydrocarbons (in the range C_2–C_{10}) and water was discovered in 1976.[4] Industrial processes, such as methanol-to-gasoline and methanol-to-olefin (MTO) conversions, have been developed since then. Methanol can be obtained from synthesis gas ($CO + H_2$), which can be produced from any gasifiable carbonaceous species, such as natural gas, coal, biomass, and waste. The reaction is catalyzed with protonated zeolites or zeotype materials, and after a kinetic induction period, hydrocarbons are formed.[2] To date, there is a consensus that the active site for MTO catalysis consists of a Brønsted acid site together with an organic reaction center also present in zeolite pores, which acts as a cocatalyst.[5–7] Thus, the active site has a hybrid organic–inorganic nature, which leads to an additional level of complexity in designing the catalyst. Each active site of the MTO process can be regarded as a well-defined supramolecular complex in which an organic component is trapped in the inorganic host (Scheme 1). This concept was described in the seminal papers of Haw and co-workers.[5,6] A thorough understanding of the interplay between the organic component and its host is of utmost importance to obtain molecular

[a] V. Van Speybroeck,[++] K. Hemelsoet,[++] K. De Wispelaere, J. Van der Mynsbrugge, B. De Sterck,[+] M. Waroquier
Center for Molecular Modeling
(Member of the QCMM Ghent-Brussels Alliance)
Ghent University
Technologiepark 903, 9052 Zwijnaarde (Belgium)
E-mail: veronique.vanspeybroeck@ugent.be

[b] Q. Qian, B. M. Weckhuysen
Inorganic Chemistry and Catalysis
Debye Institute for Nanomaterials Science
Utrecht University
Universiteitsweg 99, 3584 CG Utrecht (The Netherlands)
E-mail: b.m.weckhuysen@uu.nl

[+] Current address:
LANXESS Rubber N.V. BTR—Competence Center Technology
Haven 1009, Canadastraat 21, 2070 Zwijndrecht (Belgium)

[++] These authors contributed equally to this work.

Supporting information for this article is available on the WWW under http://dx.doi.org/10.1002/cctc.201200580.

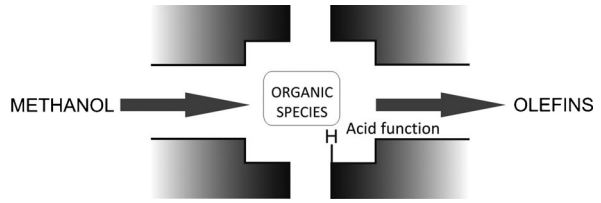

Scheme 1. View of the hybrid organic–inorganic catalyst for the MTO process.

control on the product distribution.[8] This subtle interplay between the zeolite cage, Brønsted acid site, and organic reaction center is nowadays referred to as the "hydrocarbon pool (HP) hypothesis", which was first proposed by Dahl and Kolboe[9–11] and later on proved experimentally by Haw and co-workers.[12]

Dedicated experimental studies have strengthened the concept that the HP species and their activity critically depend on the composition and topology of the catalyst material.[13–15] Catalyst and HP species must find an optimal fit to generate an active material, which is also selective toward the desired products, such as ethene or propene.[15,16] To advance in this field of research, it is essential to gain an insight into the kinetics of individual reactions and to understand how the reactivity and selectivity depend on the specific HP species. Overall kinetic data can easily be measured experimentally; however, the main challenge consists in relating the obtained information with the mechanistic knowledge of elementary reaction steps as a large number of side reactions occur. Although various aspects of the reaction are obtained easily, good comprehensive kinetic data on individual reaction steps are scarce.[17–20]

The formation and activity of various structurally different organic species trapped in a zeolite environment are assessed by using a combined experimental and theoretical approach. We demonstrate for the first that in situ UV/Vis microspectroscopy measurements can be used to deduce activation energies for the formation of organic cationic aromatics, which are inherently part of the active sites of an MTO catalyst. The studied organic compounds differ in the number of aromatic units and hence absorb light at different characteristic wavelengths. The proposed method relies on measuring the time evolution of absorption bands in experimental UV/Vis spectra. Within the area of MTH chemistry, UV/Vis microspectroscopy has principally been used to study surface adsorption and catalyst deactivation processes.[21,22] To also deduce mechanistic insight into individual reaction steps by using the optical absorption data, first-principle kinetics of elementary reactions of structurally different HP species have been determined. Recent state-of-the-art molecular modeling techniques have provided chemical accuracy for the prediction of reaction barriers and rate constants in zeolite catalysis.[23,24] The correlation between the theoretical reaction rates of individual reactions and the experimental activation energies obtained from UV/Vis spectroscopy enables the detection of governing reactions for the formation of cationic intermediates, which are trapped in the zeolite cage. We show that the correlation between measured data and individual reaction rates depends strongly on the exact nature and size of the trapped organic compound.

Active organic compounds within MTO chemistry may be defined as organic intermediates, which serve as a platform to which C_1 species can bind and from which primary olefins can dissociate. A range of methylbenzenes and other related cyclic species were identified as main intermediates for the production of olefins in various zeotype catalysts.[5,6,25–33] All mechanistic proposals for the production of olefins based on these aromatic intermediates start with a series of methylation reactions at a Brønsted acid site. The mechanism for methylation used here is the concerted pathway in which a methylating agent (e.g., methanol) is protonated and a methyl group is transferred to a ring carbon atom, which results in the formation of a cationic HP species (Scheme 2).[34–36] Various experimental ki-

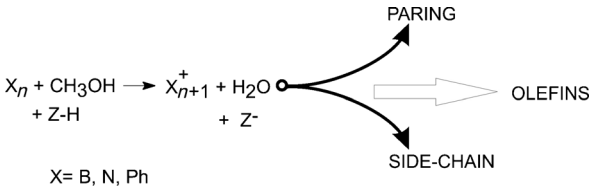

Scheme 2. Initiating methylation step for the formation of olefins from X_n, in which X stands for benzenic, naphthalenic, or phenanthrenic species and *n* is the number of methyl substitutions. Z is the zeolite.

netic data were explained with this proposal.[19,20,24,34–36] However, some other mechanistic pathways cannot be ruled out immediately, in particular the stepwise mechanism, in which surface-bound methoxy groups are formed and for which some spectroscopic evidence was also found.[34] Yet another possibility concerns the pathway in which the arene is first protonated by the Brønsted acid site and then methylated directly by a neutral methanol molecule.[37] This mechanism is relevant for the methylation of highly substituted arenes because these species have high values of proton affinities (PAs). As the primary interest of this study is to assess qualitative differences in the reactivity of various organic substrates, a full discussion on the prevailing pathway is beyond the scope of this paper and we refer to the work of Svelle and co-workers for a complete mechanistic discussion.[34]

After repeated methylations, a *gem*-methylated $X_{n+1}{}^+$ species starts the so-called "paring" cycle or "side-chain" cycle to produce olefins.[38,39] These $X_{n+1}{}^+$ species give characteristic peaks in the UV/Vis spectrum, as we will explain later. Some of them take on an active role in the operation of the supramolecular MTO catalyst by providing a platform for olefin eliminations, whereas others are rather precursors for coke formation.[40,41] As a first criterion to discriminate between active and passive HP species, the rate of methylation reactions can be used because these are initiating reaction steps in the olefin-producing cycles. Various theoretical studies have shown that methylations are key reaction steps of the process[39,40,42,43] and that, depending on the topology and organic species to be methylated, they are also rate determining.[32,44] In some cases, other reactions required for olefin formation can also be highly

activated; however, methylations remain essential steps in the overall reaction cycle.[38,39] For H-SAPO-34, Wang et al. studied the side-chain mechanism by using periodic DFT calculations and found that other reaction steps after methylations can be equally highly activated.[45,46]

As a case study for the formation and activity of organic species trapped in a confined zeolite, we selected the archetypal MTO catalyst the silicoaluminophosphate H-SAPO-34 and its aluminosilicate counterpart H-SSZ-13. These materials both have the chabazite (CHA) topology that features cages that are interconnected by much smaller windows. The opening of the cage windows is 3.8×3.8 Å and spacious elliptic cages of 6.7×10.9 Å are present (Figure 1a). Consequently, the cages can accommodate fairly large molecules; however, these cannot migrate from one cage to another and thus the molecules exiting the catalyst bed are primary MTO products with one to four carbon atoms.[47,48] H-SAPO-34 and H-ZSM-5 are currently the only two zeolite materials used in industrial MTH processes.[47,49–51]

The active HP species in CHA topologies have been established to be methylated aromatics with a varying number of methyl groups and with one or two aromatic rings.[25–28,52] In this respect, UV/Vis microspectroscopy is an ideally suited spectroscopic technique because it is highly sensitive to the presence of charged aromatic compounds and gives rise to characteristic absorption bands in the visible range. There is clear experimental evidence from earlier MTO studies that a cage containing polymethylbenzenes with a higher degree of methyl substitution becomes more active.[28,53] Methylnaphthalene compounds were found to be three times less active;[28] however, the effect of the number and precise location of methyl groups on their activity is still unclear. HP species with yet a higher number of aromatic rings are also formed but are no longer active and contribute to the aging of the catalyst.[52] Overall, this process occurs faster in H-SSZ-13 than in H-SAPO-34 owing to its higher acidity.[48,54] This was shown in the recent work of Bleken et al., in which only one parameter of the catalyst was varied at a time.[48] For the CHA framework, only the acid strength was varied by studying H-SAPO-34 and H-SSZ-13 samples with the same density of acid sites and the same crystal size. The two catalysts behave very similarly for MTO conversion, with faster deactivation and lower optimum reaction temperature for H-SSZ-13, which is expected owing to its higher acid strength. Direct kinetic measurements on such (poly)aromatic species are not possible, because they cannot be pulsed on CHA-type catalyst beds owing to diffusion limitations. To date, mechanistic insight into MTO on H-SAPO-34 has been obtained from isotopic labeling experiments,[11,26] solid-state NMR studies,[29,55] and thermal quenching of the reaction followed by a dissolution/extraction method to identify the organics trapped in zeolite pores.[25] Li and co-workers recently succeeded in observing the heptamethylbenzium cation in DNL-6, a newly synthesized SAPO-type molecular sieve with large cavities, under real MTO conversion conditions.[56] However, owing to the complexity of the mechanism, it remains a great challenge to achieve profound mechanistic insight and to identify governing reaction steps for the overall process.

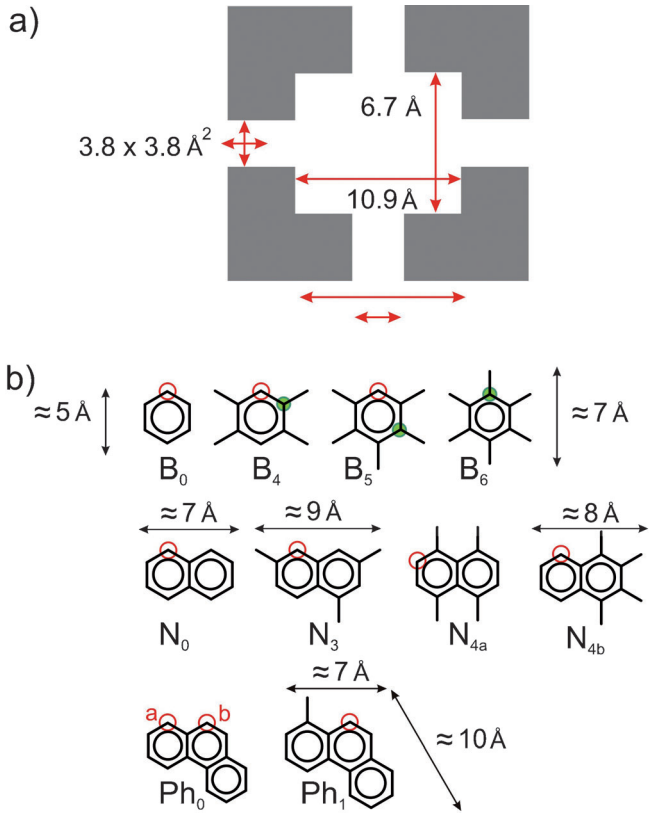

Figure 1. a) Illustration of the CHA pore with some geometrical characteristics. b) Selected HP species X_n with geometrical characteristics. The green (filled) and red (empty) circles indicate the methylation positions considered in this study, that is, methylation at an already- and nonsubstituted aromatic carbon atom.

Herein, a broad set of structurally different (poly)aromatic compounds is considered (Figure 1b). The time evolution of absorption bands in the UV/Vis spectra is followed in situ during the exposure of H-SAPO-34 and H-SSZ-13 to a stream of methanol. For each compound, first-principles kinetic methylation rates are determined, which enables the correlation of experimentally determined activation energies with individual reaction rates for organic species trapped in the confined zeolite environment.

Results and Discussion

First-principles methylation rates

For the broad set of (poly)aromatic compounds introduced in Figure 1b, first-principles methylation rates of H-SSZ-13 and H-SAPO-34 are determined to study the subtle interplay between the structure of the trapped organic species and the confining zeolite environment and its effect on the activity toward methylation. Every catalyst cage containing a trapped organic species should thus be regarded as an organic–inorganic catalyst with its own characteristics.[28,29] The notation $\{X_n\}$ is adopted to emphasize this concept, in which the catalyst is composed of the organic reaction center X_n—with n methyl substitu-

ents—in an inorganic cage with a Brønsted acid site. The activity of this complex catalyst is dictated by framework topology, framework composition, acid site strength, size, shape, and even orientation of the trapped organic compound.[57] Theoretical calculations are clearly advantageous in providing detailed insight into the effect of each of these factors on the overall activity toward methylation. The product of the methylation reaction (Scheme 2) is a cationic (poly)aromatic species, which gives characteristic peaks in the visible region of the measured UV/Vis spectra (vide infra). A schematic representation of the transition state is given in Figure 2. The methyl group is transferred in a typical S_N2 fashion through an umbrella-like inversion, and as a result a cationic X_{n+1}^+ compound is formed.[58] As mentioned in the Introduction, some other mechanistic proposals for the methylation exist. Although a detailed study of these is beyond the scope of this article, the work of Svelle et al. provides a complete mechanistic discussion.[34]

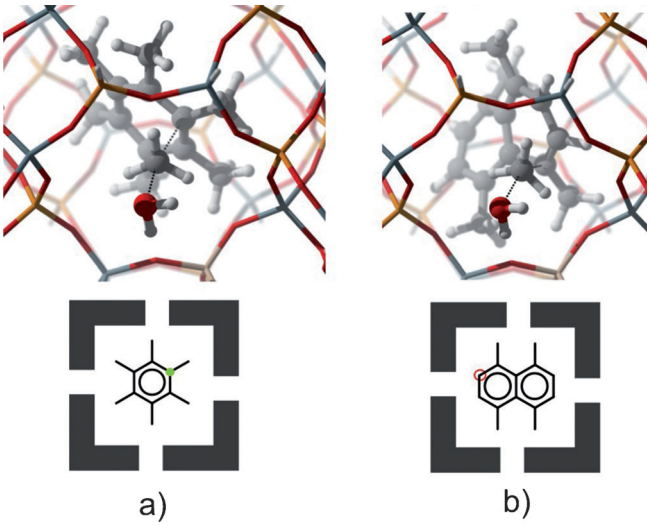

Figure 2. Transition state geometries for the methylation of $\{B_6\}$ and $\{N_{4a}\}$ species in H-SAPO-34.

The methylation rates at 555 K, activation barriers, and pre-exponential factors obtained between 500 and 630 K for the selected HP species are given in Table 1 for both H-SAPO-34 and H-SSZ-13 catalysts. For the series of (poly)methylbenzenes, methylations at both an unsubstituted and a substituted carbon atom are considered. The notation $X_{n,g}$ is used to indicate *ipso*-methylations leading to a *gem*-methylated species.

Even without going into detail, it is immediately clear that the reaction rates vary considerably—by 6 orders of magnitude—depending on the specific organic compound in the zeolite cage. To thoroughly understand the impact of the various factors contributing to these overall kinetic results, a series of additional simulations were undertaken, which allow one to discriminate between the number of aromatic rings and the number of methyl substitutions on the organic compound, zeolite composition, and cage restrictions.

The intrinsic effect of the number of aromatic rings on the methylation rates was assessed by calculating the Gibbs free energies for the methylation reactions in the gas phase in which a protonated methanol was used as the reactant. In the gas phase, the unscreened CH_3OH^+ methylating agent is so reactive that every other effect induced by the (poly)aromatic substrate is masked. To mimic the electrostatic stabilization provided by the zeolite catalyst, the system was embedded in a continuum characterized by a specific dielectric constant by using an implicit solvent model (in this case water). The free energies of activation and reaction free energies are shown in Figure 3a (results indicated by "without zeolite cage"). During methylation, the aromaticity is broken and a carbenium ion is formed. Gibbs free energies of the reaction amount to 0, −30, and −35 kJ mol^{-1} for benzene, naphthalene, and phenanthrene (Ph_{0b}), respectively, and are determined by the degree to which the positive charge can be delocalized. Without consideration of the zeolite confinement effect, the following reactivity trend is predicted: $Ph_{0b} > N_0 > B_0$ and Ph_{0a} less reactive than Ph_{0b} (results indicated with "without zeolite cage" in Figure 3a). This sequence is in line with Clar's π-electron sextet stability model, which states that the reactivity of polycyclic aromatic hydrocarbons can be deduced by the maximum number of aromatic sextets that can be drawn for a given structure.[59]

If the zeolite environment is taken into account, benzene remains the less reactive species, followed by Ph_{0b} and Ph_{0a} and finally N_0 has the lowest free energy of activation (Figure 3a, results indicated with "H-SSZ-13"). This set of simulations enables the assessment of the reactivity of the $\{X_0\}_{H\text{-}SSZ\text{-}13}$ supramolecular cage toward methylation. Maximum variations in activation barriers amount to 30 kJ mol^{-1}, and reaction rates vary with 2 orders of magnitude (Table 1, rows B_0, N_0, Ph_{0a}, and Ph_{0b}).

A second set of simulations is designed to assess the effect of the number and position of methyl groups on the reactivity sequence within the $\{B_n\}$ series. The reaction barriers and reac-

Table 1. Rate constants at 555 K (k), pre-exponential factors (A), and activation barriers (E_a) for methylation reactions.[a,b]

	H-SAPO-34			H-SSZ-13		
	$k_{555\,K}$ [s^{-1}]	A [s^{-1}]	E_a [kJ mol^{-1}]	$k_{555\,K}$ [s^{-1}]	A [s^{-1}]	E_a [kJ mol^{-1}]
B_0	2.0×10^{-3}	2.9×10^{11}	150.5	2.5×10^{-1}	6.9×10^{12}	142.8
B_4	1.3×10^{0}	1.6×10^{12}	128.2	6.0×10^{2}	1.3×10^{12}	99.4
$B_{4,g}$	1.4×10^{0}	3.6×10^{12}	131.8	1.1×10^{3}	4.2×10^{12}	101.6
B_5	3.8×10^{1}	5.4×10^{12}	118.5	7.3×10^{3}	4.9×10^{12}	93.8
$B_{5,g}$	8.3×10^{0}	1.7×10^{13}	130.8	1.9×10^{5}	1.5×10^{13}	84.1
$B_{6,g}$	8.3×10^{2}	5.7×10^{12}	104.5	6.5×10^{5}	1.1×10^{13}	77.3
N_0	3.0×10^{-1}	5.3×10^{12}	140.8	1.5×10^{2}	4.3×10^{12}	111.0
N_3	2.3×10^{2}	7.3×10^{12}	111.6	3.5×10^{5}	2.5×10^{13}	83.5
N_{4a}	1.2×10^{0}	5.1×10^{12}	134.2	3.4×10^{3}	5.0×10^{12}	97.4
N_{4b}	–	–	–	3.9×10^{2}	1.6×10^{13}	112.7
Ph_{0a}	1.8×10^{-1}	1.3×10^{13}	147.3	7.9×10^{1}	2.5×10^{13}	122.3
Ph_{0b}	9.4×10^{-2}	4.3×10^{12}	145.1	3.2×10^{0}	3.3×10^{12}	127.5
Ph_1	1.9×10^{-1}	5.0×10^{12}	142.5	9.7×10^{0}	1.6×10^{12}	119.9

[a] The notation $X_{n,g}$ is used to indicate *ipso*-methylations leading to a *gem*-methylated species; [b] For N_{4b}, no meaningful results could be obtained because methanol was pushed out of the H-SAPO-34 cage during optimization.

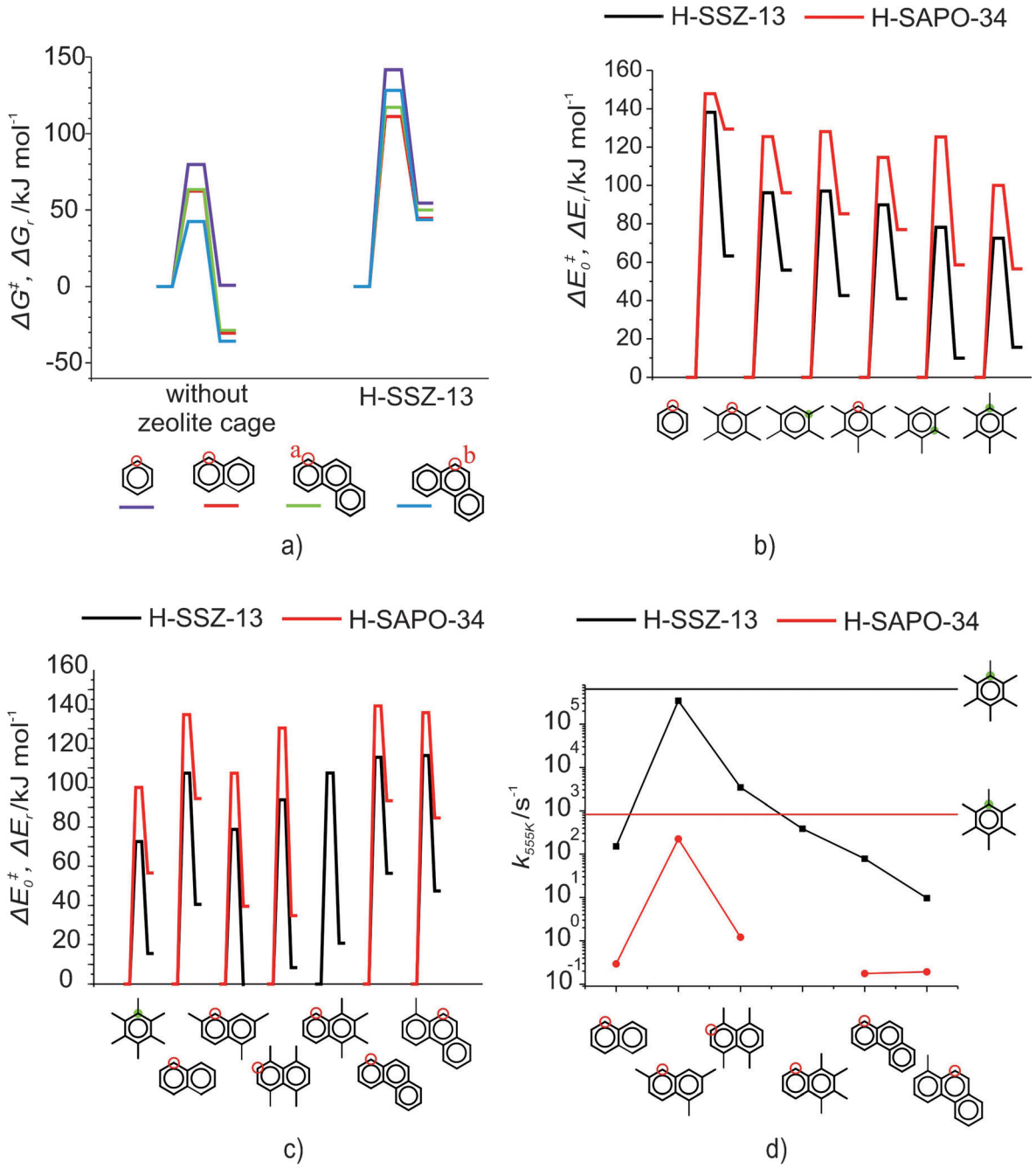

Figure 3. a) Free energies of activation $\Delta G^{\ddagger}$ and reaction free energies ΔG_r at 298 K for various polyaromatic hydrocarbons with no methyl substituents and calculated with and without the inclusion of the zeolite molecular environment. b–c) Barrier heights $\Delta E_0^{\ddagger}$ and reaction energies ΔE_r including zero-point vibrational corrections for the {B_n}, {N_n}, and {Ph_n} series with varying number of methyl groups. d) Intrinsic reaction rate coefficients $k_{555\,K}$ calculated at 555 K for various methylation reactions. All values are calculated by using B3LYP/DGTZVP-D energies.

tion energies at 0 K for all studied B_n species both in H-SSZ-13 (——) and H-SAPO-34 (——) are shown in Figure 3b, and the kinetic data are reported in Table 1. The transition state for the methylation of {B_6} is shown in Figure 2a. Within the {B_n} series, the barrier decreases systematically with an increasing number of methyl substitutions and the rate constant increases by approximately 5 orders of magnitude with highest values for penta- and hexamethylbenzene in accordance with earlier experimental results, which designated these species as the most active HP species within the CHA topology.[28,53] The HP species within the {B_n} series are not subject to any transition state selectivity for the studied methylation reactions.[29,53,60–62] Current results within the CHA topology are in stark contrast with the detected transition state selectivity in the other industrially important catalyst for MTO, that is, ZSM-5, in which the reaction barrier increases from four methyl groups owing to limited space available at the intersections of the straight and sinusoidal channels in the medium-pore MFI topology.[19,63] We have also calculated the *ipso*-methylation rates for some species and found that *ipso*-methylations on the higher methylated ben-

zene species were not faster than normal methylations (cf. rows B_4 and $B_{4,g}$ with rows B_5 and $B_{5,g}$), despite possible additional stabilization due to hyperconjugation. If the rates of *ipso*- and normal methylations are compared, one needs to compare transition states and corresponding prereactive complexes with similar orientations in the cage. We illustrate this concept for reactions B_4 and $B_{4,g}$ and for B_5 and $B_{5,g}$. For these reactions, several transition states could be located, which differ merely by the orientation of the prereactive complex in the zeolite cage. The results listed in Table 1 refer to the reaction path with similar prereactive complexes of reactions B_4 and $B_{4,g}$ as well as reactions B_5 and $B_{5,g}$. Only in this case a comparison between normal and *ipso*-methylations is justified as we calculate intrinsic reaction rate coefficients. In an alternative reaction path, the prereactive complexes of normal and *ipso*-methylations differ by a rotation of the aromatic compound of 120° over the axis perpendicular to the aromatic plane. Owing to this rotation, the prereactive complexes of the studied *ipso*-methylations are systematically less stable than those of normal methylations. An energy diagram for B_4 and $B_{4,g}$ in H-SAPO-34 is depicted in Figure S4 of the Supporting Information. The rotated prereactive complex (referred as $B_{4,g}'$) is 111 kJ mol^{-1} less stable than the originally considered complex, and as a result the intrinsic kinetics is slightly less activated (120.8 kJ mol^{-1}). These results show that aromatic HP species cannot rotate freely inside the CHA cage and that a careful analysis of prereactive complexes together with the intrinsic reaction rates is indispensable to assess the relative importance of competing reactions. For the $\{B_n\}$ series for which transition state selectivity is not important, the reactivity trend is dictated by the stability of the formed carbenium ions within the zeolite.[46] A possible method to rationalize these stabilities is based on gas phase basicities.[33,64] The calculated PAs of the formed carbenium ions are given in Table S1. Although a clear correlation between the PA values and activation barriers is present, no linear relation can be established because the degree of confinement within the cage needs to be taken into account. The reaction energies and activation barriers are systematically lower within H-SSZ-13 because this material is more acidic than H-SAPO-34.[41] The difference in acidity was quantified both experimentally and theoretically by measuring the shift in OH stretching frequency upon adsorption of CO.[63,65] The difference in acidity of both materials is also reflected in the calculated deprotonation energies of H-SAPO-34 and H-SSZ-13, which differ by approximately 20 kJ mol^{-1} (Table S2). The previous set of simulations enables the evaluation of the reactivity of the $\{B_n\}_{\text{H-SSZ-13/H-SAPO-34}}$ cage toward methylation. The variations in activation barriers induced by additional methyl groups positioned on the ring are substantial and amounts to approximately 60 kJ mol^{-1}. These structural modifications on the organic species outweigh the effect induced by altering the number of aromatic rings. As a result, the methylation rates vary with at least 6 orders of magnitude (rows B_0, B_4, $B_{4,g}$, B_5, $B_{5,g}$, and $B_{6,g}$).

A last set of simulations is designed to assess the activity toward methylation for a supramolecular cage $\{X_n\}$, in which X = N or Ph and the number *n* of methyl substitutions can vary from 1 to 4. Thus, the combined effect of multiple aromatic rings, various methyl substitutions, and the confined environment on the activity of the organic compound is assessed. The cage with hexamethylbenzene is the most active and therefore all new kinetic data are referred to the $\{B_{6,g}\}$ cage. The results are plotted in Figure 3c and d and listed in Table 1. The zeolite cage $\{N_0\}$ with an unsubstituted naphthalenic species has a relatively high barrier (107 and 137 kJ mol^{-1} in H-SSZ-13 and H-SAPO-34, respectively), and this value remains rather stable up to three methyl substitutions.[40,41] Interestingly, for a cage with a naphthalenic compound bearing three methyl substitutions $\{N_3\}$, the barrier drops to 79 kJ mol^{-1} in H-SSZ-13 and 107 kJ mol^{-1} in H-SAPO-34, which is only slightly higher than the values for the most reactive HP compound $\{B_{6,g}\}$. If four, five, or six methyl substituents are present, the reaction barriers increase successively, the reactions become more endothermic, and the reaction rates decrease, which gives clear evidence for transition state selectivity for the more substituted naphthalenic species. The steric constraints imposed by the CHA cage are also visible from the 3D figure of the optimized transition state for compound N_{4a} (Figure 2b). The reaction rates show similar trends and vary with approximately 5 orders of magnitude (Figure 3d). The variations in the pre-exponential factors are rather modest and the reactivity sequence is dictated by activation barriers. From acid digestion experiments on an H-SAPO-34 catalyst, it was observed that naphthalene rings never contain more than four methyl groups; it was however impossible to deduce the activity in terms of the precise location of methyl groups.[5,6,28] Our results show that a cage with an N_4 species with all four methyl groups on one ring is less reactive and subject to severe steric constraints and does not behave as a confined tetramethylbenzyl species. However, the trapped N_3 species with the methyl groups equally distributed among two rings is as reactive as the trapped B_6 species. Phenanthrene-type species have methylation rates at least 1 order of magnitude smaller (Figure 3d). These species do not operate as active centers for the MTO process. This was confirmed by ^{13}C scrambling experiments, in which labeled methanol was fed. Labeled carbon atoms scrambled substantially into di-, tri-, and tetra-methylnaphthalene rings, whereas phenanthrene and pyrene did not scramble at all.[28] This set of simulations point clearly toward the transition state selectivity of some substituted naphthalenic compounds, although the lower methylated naphthalenic compounds can be as reactive as the most active organic species, that is, hexamethylbenzene.

Activation energies of formation from in situ spectroscopy

To correlate the theoretical observations on the activity toward methylation with experimental data, we used in situ UV/Vis microspectroscopy under realistic working conditions for the catalyst materials under study. A new analysis method is proposed here to deduce activation energies of the formation of the crucial cationic HP intermediates (X_{n+1}^+ species), which give rise to characteristic absorption bands in the optical spectra. H-SAPO-34 (58×58×58 μm) and H-SSZ-13 (40×40×40 μm) zeolite crystals are placed on the heating stage of an in situ

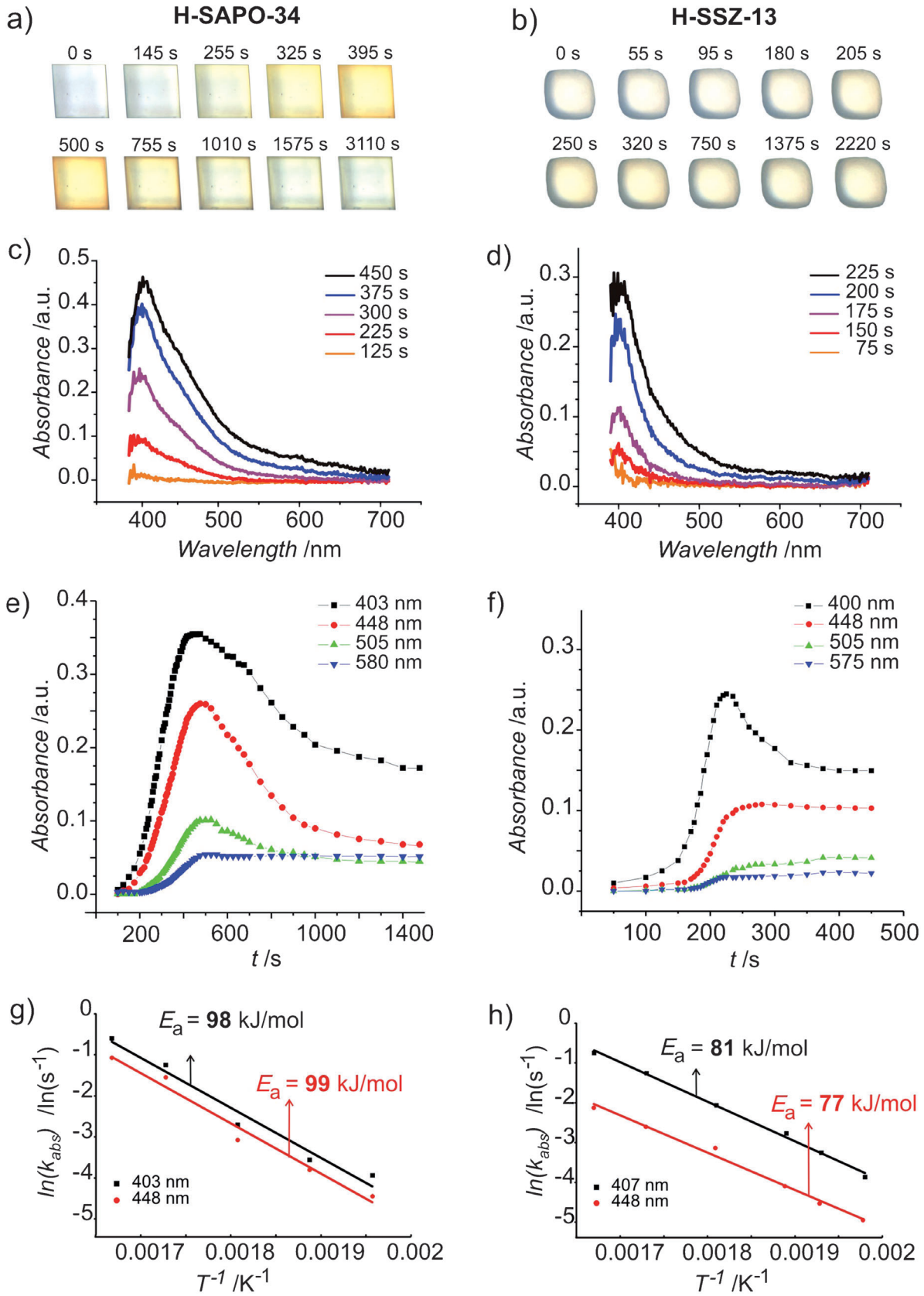

Figure 4. a–b) Optical microphotographs taken at a 2 μm spot in the center of the crystals, c–d) selection of time-resolved in situ UV/Vis spectra, e–f) time development of the Gaussian functions taken during the MTO reaction at 553 K. g–h) Arrhenius plots derived from the temporal evolution of various absorption bands in the temperature range 500–600 K with indication of the slope.

cell and exposed to a stream of methanol vapor in the reaction temperature range of 500–600 K. Optical microphotographs taken during the MTO reaction at 553 K on H-SAPO-34 and H-SSZ-13 are shown in Figure 4a and b. For H-SAPO-34, a strong yellow coloration is observed along the edges of the crystal, with maximal color intensity around 500 s. Subsequently, the sample becomes more translucent, an effect that depends on the reaction temperature.[21] Some authors have reported previously that for H-SAPO-34, no blackening is observed in the analysis of optical microphotographs, which indicates that the coke is formed predominantly inside zeolite pores.[21] For H-SSZ-13, the growth of absorption bands proceeds substantially faster, as indicated by the time intervals in Figure 4b. At 553 K, the growth of a strong absorption band at 400 nm is visible clearly, which indicates the presence of highly methylated benzenium cations (Figure 4c and d).[21,22,66] With time on stream, a second absorption band appears at 480 nm, and later, a weak and broad absorption band grows at higher wavelengths around 580 nm, which is evident in the case of the more acidic H-SSZ-13 material at particular temperatures. In Figure S2, the in situ UV/Vis profiles are given for methanol reaction at 553 K with longer reaction time, whereas in Figure S3, the results of methanol reaction at 528 K are shown. Both temperature and catalyst composition affect the behavior of the spectra in a subtle manner. These subtle balances have also been studied by Bleken et al. at slightly different conditions.[48] Also, Mores et al. found a subtle effect of temperature on the absorbance spectra for H-ZSM-5 crystals with different Brønsted acidities.[22] The detailed effect on the process temperatures clearly needs further investigation. The large variety of carbonaceous species during the MTO reaction is reflected by overlapping absorption bands, and more quantitative insight can be obtained from the deconvolution of these optical spectra. Four Gaussian bands—with band maxima approximately at 400, 450, 505, and 580 nm—are necessary to reconstruct the experimental UV/Vis spectra, whereas a wide absorption band with a maximum at 700 nm is used to correct the baseline and a band at 670 nm has a very small contribution to the overall shape of the spectra. The band position and width of the Gaussian functions are summarized in Table 2. A representative set of deconvoluted spectra is shown in Figure 5, and the same set of Gaussian bands was chosen for all H-SAPO-34 and H-SSZ-13 spectra to guarantee a systematic analysis. Notably, some spectra were rather challenging to fit and a maximum shift of 4 nm was allowed, which is similar to previous work involving H-ZSM-5.[22]

Table 2. Summary of the Gaussian functions used for deconvolution of the in situ UV/Vis spectra of H-SAPO-34 and H-SSZ-13 crystals.

	Gaussian bands[a] [nm]					
H-SAPO-34	403 (31)	448 (42)	505 (46)	580 (50)	670 (65)	700 (800)
H-SSZ-13	400 (31)	448 (45)	505 (48)	575 (60)	665 (65)	700 (800)

[a] Band positions (widths in parentheses).

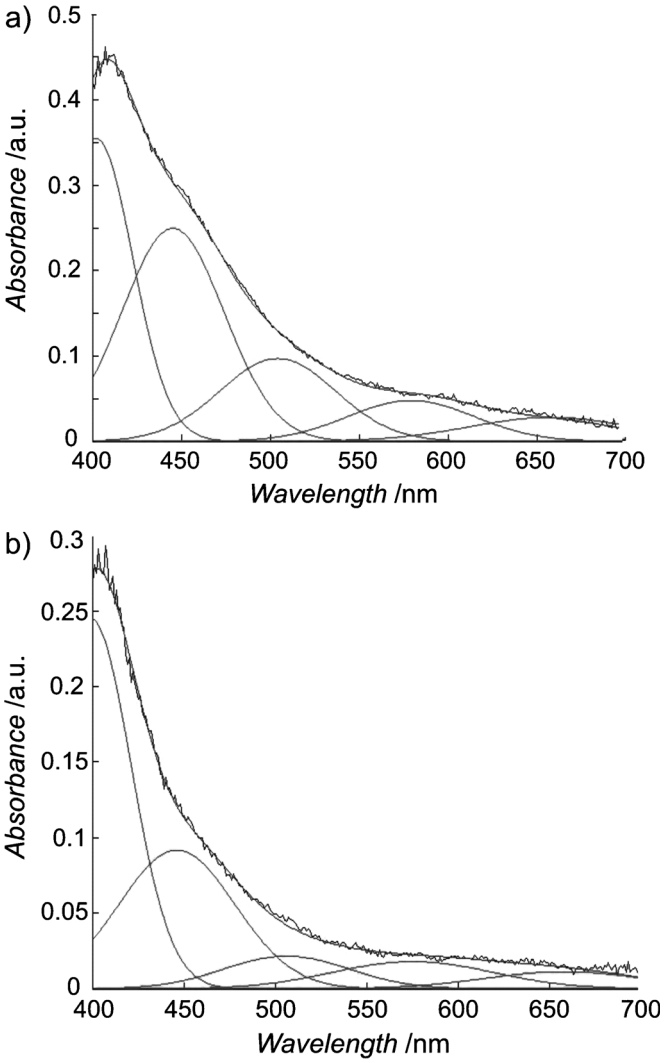

Figure 5. Illustration of the deconvolution method applied to the UV/Vis spectra after a) 450 (for H-SAPO-34) and b) 225 (for H-SSZ-13) s of the MTO reaction at 553 K.

For each band, the evolution of the maximal absorbance as a function of time was monitored at different temperatures. The rapidly increasing regions in the absorbance (A) versus time (t) curves (see Figure 4e and f) that follow first-order kinetics were selected and fitted to the equation $\ln(A_{max}-A) = \ln A_{max} - kt$. We thus corrected for an induction period at the beginning and for the occurrence of secondary reactions near the end of the process; the regions between $0.2A_{max}$ and $0.5A_{max}$ for H-SAPO-34 and between $0.3A_{max}$ and $0.7A_{max}$ for H-SSZ-13 were used. The time interval (Δt) of the first-order reaction region is then used to determine an absorption rate constant k_{abs} ($k_{abs} = 5/\Delta t$, in which the time interval is expressed in units of 5 s), and $\ln(k_{abs})$ as a function of $1/T$ is depicted in Figure 4g and h. The slope of these Arrhenius curves is denoted as the activation energy of formation of the charged (poly)aromatic species responsible for the increase of the absorption band in the UV/Vis spectra. By using this method, the activation energy for the growth of the 400 nm band was determined to be 98 and 81 kJ mol^{-1} for H-SAPO-34 and H-SSZ-13, respectively (Figure 4g and h). The obtained accuracy of the

derived formation activation energies is validated for the 400 nm band of H-SAPO-34 (see the Supporting Information) and approximates 10 kJ mol^{-1}, which is similar to the accuracy of the theoretical predictions.

These values cannot straightforwardly be assigned to activation energies of one particular reaction because of the complexity of the methanol conversion mechanism. However, if methylation reactions are rate-determining steps for the formation of (poly)aromatic cations, a strong correlation is expected between the theoretical rates of methylation and the experimentally derived activation barriers for the growth of absorption bands.

To explore such a correlation, it is important to assess which structurally different HP species contribute to various UV/Vis absorption bands. By using time-dependent DFT calculations, we determined for each cationic HP species (X_{n+1}^{+}) the vertical electronic excitation energy, which enabled the construction of the assignment scale given in Figure 6 (Table S3). Thus, higher methylated benzenium ions, such as B_6^{+} and B_7^{+} species, contribute to the 400 nm absorption band. There is a good correlation between the theoretical methylation activation energies of {B_6} (e.g., 105 and 77 kJ mol^{-1} in H-SAPO-34 and H-SSZ-13, respectively, in Table 1) and the experimental formation activation energies of the 400 nm absorption band. Furthermore, both theoretical and experimental activation energies predict a difference of approximately 20–30 kJ mol^{-1} between H-SAPO-34 and H-SSZ-13. This confirms that methylation reactions are the governing reaction steps in the formation process of the cationic highly methylated benzenic compounds, which absorb around 400 nm. The formation activation energies of the 450 nm band were experimentally determined to be 99 and 77 kJ mol^{-1} for H-SAPO-34 and H-SSZ-13, respectively, and are quite similar to the values for the 400 nm absorption band (Figure 4 g and h). According to the theoretically determined assignment scale, cationic naphthalenic compounds containing up to four methyl groups contribute to this absorption band (computed excitation energies around 470 nm) whereas the higher methylated ones predominantly absorb light at substantially higher wavelengths around 550 nm. Theoretically, some of the lower methylated naphthalenic species (Table 1, reaction N_3) are as reactive as the benzenic ones, whereas higher methylated species demonstrate higher activation energies for methylations. For the higher absorption bands (i.e., 505 and 580 nm), the temporal evolution of the bands is hard to monitor because their growth is limited. Therefore, no reliable formation–activation barriers can be derived for these bands and the link with the theoretical methylation barriers cannot be made. Methylation reactions are thus not rate-determining steps for the growth of larger coke precursors.

Conclusions

We have applied a combined spectroscopic and theoretical approach to obtain insight into the formation and nature of active sites and related intermediates for the conversion of methanol over solid acid catalyst materials. The catalyst at hand has a hybrid organic–inorganic nature in which confined organic compounds, Brønsted acid site, and the inorganic zeolite cage are entangled in a subtle manner. The formation and activity of structurally different organic compounds have been monitored by using a unique approach relying on first-principle calculations on elementary reactions, which are rate determining in the overall reaction cycle on one hand and in situ UV/Vis microspectroscopy while exposing the catalyst samples to a stream of methanol on the other. In our study, zeotype materials with the CHA topology are taken as a case study for the confined host environment and various (poly)aromatic compounds represent trapped cocatalytic species. The organic compounds provide a platform to which C_1 species can bind and from which product hydrocarbon species can dissociate. Methylation reactions can be regarded as essential reaction steps in the overall catalytic cycle. Therefore, first-principle methylation rates have been determined, which show that the activity toward methylation critically depends on the structure of the organic compound, the cage restrictions, and the catalyst composition. Rates at actual working temperatures vary by at least 6 orders of magnitude, which provides solid evidence for the subtle interplay of various components constituting the catalyst material. If steric constraints are less important as in the benzene series, the largest effect on the reaction rate is induced by the number of methyl groups on

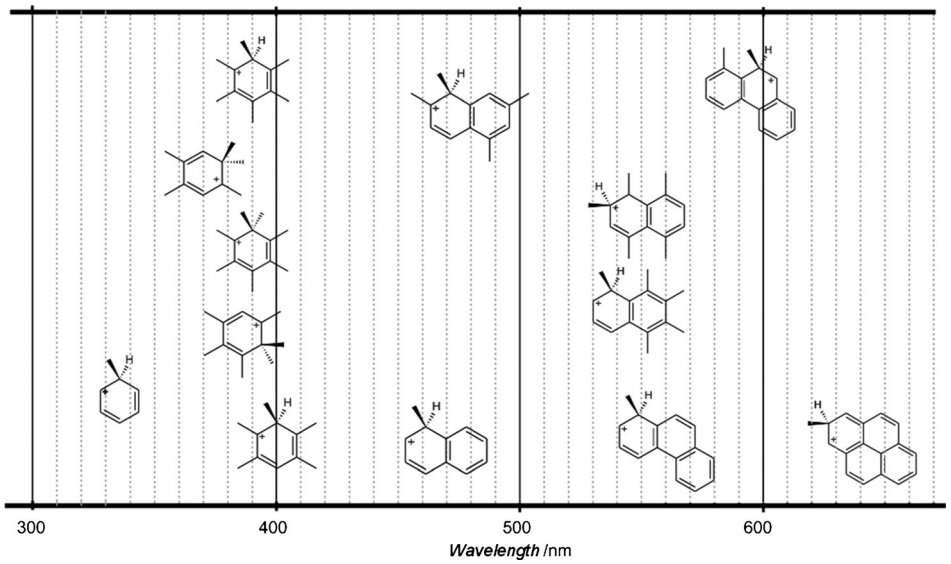

Figure 6. First time-dependent DFT excitation energies (in nm) of the gas phase charged HP compounds calculated at the B3LYP/DGTZVP level of theory (see also Table S3).

the aromatic core, which leads to 6 orders of magnitude acceleration in the reaction rate. For organic compounds bearing more aromatic rings, transition state selectivity was observed from four methyl groups, which results in methylation rates that are substantially lower than those of the most active compounds. The number of methyl groups governs not only the reaction rate but also their precise location among the aromatic rings. As expected, the effect of the zeolite composition is also visible in the overall reaction rates, which are about 3 orders faster in H-SSZ-13 than in H-SAPO-34.

In addition to assessing the activity toward methylation by using theoretical simulations, we followed the formation of the cationic (poly)aromatic species by using in situ UV/Vis microspectroscopy because they give characteristic peaks in the visible region of the spectrum. A correlation could be established between the methylation activation barriers for the most active species and the formation–activation barriers deduced by using UV/Vis microspectroscopy. In particular, benzenic and lower methylated naphthalenic compounds were established as the most active compounds toward methylation, and the formation of these species can be linked with the growth of absorption bands at 400 and 450 nm. The larger compounds bearing more aromatic units behave as coke precursors rather than active compounds in the MTO chemistry. The study presents a novel approach to obtain fundamental insight into the functioning of a complex catalyst material of high economic interest.

Computational Methods

For various key reactions in the MTO process, the effect of topology on the chemical kinetics was unambiguously proven to be of utmost importance both experimentally and theoretically.[14,42,57] Various methodologies can be theoretically adopted to account for the material's topology. One possibility is the use of periodic calculations in which one or several unit cells are included explicitly in the computational model.[23,45,46] Sauer and co-workers showed that enthalpy barriers for individual reactions in heterogeneous catalysis could be calculated with near chemical accuracy by using a computationally expensive method.[23] Although this work can be considered as a landmark study, the methodology is computationally too demanding to be routinely used in a large set of individual reaction steps. Here, we adopted a large cluster approach for which we showed that it could provide chemical kinetics with very high accuracy and which is computationally attractive.[24] All calculations were performed on a 44T finite zeolite cluster cutout of the CHA crystallographic structure of H-SAPO-34 and H-SSZ-13.[42,67,68] From a computational technical point of view, the location of transition states and interpretation of normal modes are substantially simpler in a cluster model than in a periodic approach.[69,70] Starting structures of 44T clusters were constructed with Zeobuilder,[71] and optimizations were performed at the ONIOM(B3LYP/DGTZVP:MNDO) level with the Gaussian 03 package.[72] The high DFT level was used for an embedded 6T cluster—constructed symmetrically around the acidic proton—and the organic guest molecules. For related reactions, interesting complementary benchmark studies are available in the literature, making use of other contemporary methods.[73–75] A representation of the 44T cluster model has been depicted in Figure S1. The outer hydrogen atoms were constrained to prevent unphysical deformations of the cluster during the geometry optimization. Frequency calculations were performed by using a partial Hessian vibrational analysis.[76,77] Energy refinements were performed by using the B3LYP/DGTZVP-D level, which included dispersion interaction corrections.[78] The rate coefficients were determined by using unimolecular transition state theory because it is assumed that the considered aromatics are unable to leave the CHA cages and the methanol molecules are abundant in the catalyst. By using this approach, the intrinsic kinetic parameters, that is, activation energy and preexponential factor, are obtained.[24,79] The in-house-developed code TAMKIN was used for the kinetic analysis.[80] Electronic excitations of the gas phase HP species were computed with time-dependent DFT[81–85] at the B3LYP/DGTZVP level of theory by using B3LYP/DGTZVP-optimized geometries. Computed excitation energies are reported in wavelength units (nm) to allow a clear comparison with the experimental data.

Experimental Section

The as-synthesized H-SAPO-34 and H-SSZ-13 crystals under study had crystal sizes of $58\times58\times58$ and $40\times40\times40$ μm, respectively. Their synthesis method is reported elsewhere.[86–88] The (Al + P)/Si and Si/Al ratios were 4.9 and 17.7, respectively. Herein large size crystals were used, which is warranted because the chemistry is very similar to that of real zeolites, but much better controlled.[89,90] The importance of framework defects on the structure–activity relationship for MTH chemistry and the desilication process was studied for ZSM-5 zeolites.[91–93] Barbera et al. pointed toward the crucial role of internal silanol groups in the deactivation behavior of the catalyst materials whereas the activity typically depends on the acid site density.[91]

The crystals were heated on the heating stage of an in situ cell (Linkam FTIR600) equipped with a temperature controller (Linkam TMS 93). The calcined crystals were first heated to 673 K at 15 K min^{-1}, then to 823 K at 5 K min^{-1}, at which temperature they were kept for 1 h under an N_2 atmosphere. Subsequently, the temperature was brought to the required reaction temperature at the rate of 15 K min^{-1} after which the N_2 flow was introduced to a methanol solution, thereby acting as carrier gas. The UV/Vis microspectroscopy measurements were performed by using an Olympus BX41 upright microscope with a 50×0.5 NA high working distance microscope objective lens. A 75 W tungsten lamp was used for illumination. In addition, the microscope had a 50/50 double viewpoint tube, which accommodated a charge-coupled device video camera (ColorView IIIu, Soft Imaging System GmbH) and an optical fiber mount. A 200 μm core fiber connected the microscope to a charge-coupled device UV/Vis spectrometer (AvaSpec-2048TEC, Avantes BV).

Acknowledgements

We thank the Fund for Scientific Research-Flanders (FWO), the Research Board of Ghent University (BOF) and BELSPO in the frame of IAP/6/27 for financial support. Funding was also received from the European Research Council under the European Community's Seventh Framework Programme (FP7 (2007–2013) ERC grant agreement number 240483). B.M.W. acknowledges financial support from the National Research School Combination-Catalysis and NWO-CW (Top Grant). Zoran Ristanovic (Utrecht University) is thanked for assistance with the analysis of the UV/Vis spectra, whereas Prof. J. Kornatowski (Max Planck Institute,

Mülheim) and E. Eilertsen (University of Oslo) are acknowledged for providing zeolite crystals.

Keywords: computational methods · heterogeneous catalysis · kinetics · in situ spectroscopy · zeolites

[1] P. N. R. Vennestrøm, C. M. Osmundsen, C. H. Christensen, E. Taarning, *Angew. Chem.* **2011**, *123*, 10686 – 10694; *Angew. Chem. Int. Ed.* **2011**, *50*, 10502 – 10509.
[2] M. Stocker, *Microporous Mesoporous Mater.* **1999**, *29*, 3 – 48.
[3] U. Olsbye, S. Svelle, M. Bjørgen, P. Beato, T. V. W. Janssens, F. Joensen, S. Bordiga, K. P. Lillerud, *Angew. Chem.* **2012**, *124*, 5910 – 5933; *Angew. Chem. Int. Ed.*, **2012**, *51*, 5810 – 5831.
[4] C. D. Chang, A. J. Silvestri, *J. Catal.* **1977**, *47*, 249 – 259.
[5] J. F. Haw, D. M. Marcus, *Top. Catal.* **2005**, *34*, 41 – 48.
[6] J. F. Haw, W. G. Song, D. M. Marcus, J. B. Nicholas, *Acc. Chem. Res.* **2003**, *36*, 317 – 326.
[7] D. Lesthaeghe, V. Van Speybroeck, G. B. Marin, M. Waroquier, *Angew. Chem.* **2006**, *118*, 1746 – 1751; *Angew. Chem. Int. Ed.* **2006**, *45*, 1714 – 1719.
[8] A. Bhan, E. Iglesia, *Acc. Chem. Res.* **2008**, *41*, 559 – 567.
[9] I. M. Dahl, S. Kolboe, *Catal. Lett.* **1993**, *20*, 329 – 336.
[10] I. M. Dahl, S. Kolboe, *J. Catal.* **1994**, *149*, 458 – 464.
[11] I. M. Dahl, S. Kolboe, *J. Catal.* **1996**, *161*, 304 – 309.
[12] W. G. Song, D. M. Marcus, H. Fu, J. O. Ehresmann, J. F. Haw, *J. Am. Chem. Soc.* **2002**, *124*, 3844 – 3845.
[13] Z. M. Cui, Q. Liu, Z. Ma, S. W. Bian, W. G. Song, *J. Catal.* **2008**, *258*, 83 – 86.
[14] Z. M. Cui, Q. Liu, W. G. Song, L. J. Wan, *Angew. Chem.* **2006**, *118*, 6662 – 6665; *Angew. Chem. Int. Ed.* **2006**, *45*, 6512 – 6515.
[15] S. Svelle, F. Joensen, J. Nerlov, U. Olsbye, K. P. Lillerud, S. Kolboe, M. Bjorgen, *J. Am. Chem. Soc.* **2006**, *128*, 14770 – 14771.
[16] S. Teketel, U. Olsbye, K. P. Lillerud, P. Beato, S. Svelle, *Microporous Mesoporous Mater.* **2010**, *136*, 33 – 41.
[17] S. Svelle, P. A. Ronning, S. Kolboe, *J. Catal.* **2004**, *224*, 115 – 123.
[18] S. Svelle, P. O. Ronning, U. Olsbye, S. Kolboe, *J. Catal.* **2005**, *234*, 385 – 400.
[19] J. Van der Mynsbrugge, M. Visur, U. Olsbye, P. Beato, M. Bjorgen, V. Van Speybroeck, S. Svelle, *J. Catal.* **2012**, *292*, 201 – 212.
[20] I. M. Hill, S. Al Hashimi, A. Bhan, *J. Catal.* **2012**, *285*, 115 – 123.
[21] D. Mores, E. Stavitski, M. H. F. Kox, J. Kornatowski, U. Olsbye, B. M. Weckhuysen, *Chem. Eur. J.* **2008**, *14*, 11320 – 11327.
[22] D. Mores, J. Kornatowski, U. Olsbye, B. M. Weckhuysen, *Chem. Eur. J.* **2011**, *17*, 2874 – 2884.
[23] S. Svelle, C. Tuma, X. Rozanska, T. Kerber, J. Sauer, *J. Am. Chem. Soc.* **2009**, *131*, 816 – 825.
[24] V. Van Speybroeck, J. Van der Mynsbrugge, M. Vandichel, K. Hemelsoet, D. Lesthaeghe, A. Ghysels, G. B. Marin, M. Waroquier, *J. Am. Chem. Soc.* **2011**, *133*, 888 – 899.
[25] B. Arstad, S. Kolboe, *Catal. Lett.* **2001**, *71*, 209 – 212.
[26] B. Arstad, S. Kolboe, *J. Am. Chem. Soc.* **2001**, *123*, 8137 – 8138.
[27] W. G. Song, J. F. Haw, J. B. Nicholas, C. S. Heneghan, *J. Am. Chem. Soc.* **2000**, *122*, 10726 – 10727.
[28] W. G. Song, H. Fu, J. F. Haw, *J. Phys. Chem. B* **2001**, *105*, 12839 – 12843.
[29] W. G. Song, H. Fu, J. F. Haw, *J. Am. Chem. Soc.* **2001**, *123*, 4749 – 4754.
[30] A. Sassi, M. A. Wildman, H. J. Ahn, P. Prasad, J. B. Nicholas, J. F. Haw, *J. Phys. Chem. B* **2002**, *106*, 2294 – 2303.
[31] M. Bjorgen, F. Bonino, S. Kolboe, K. P. Lillerud, A. Zecchina, S. Bordiga, *J. Am. Chem. Soc.* **2003**, *125*, 15863 – 15868.
[32] M. Bjorgen, U. Olsbye, D. Petersen, S. Kolboe, *J. Catal.* **2004**, *221*, 1 – 10.
[33] M. Bjorgen, F. Bonino, B. Arstad, S. Kolboe, K. P. Lillerud, A. Zecchina, S. Bordiga, *ChemPhysChem* **2005**, *6*, 232 – 235.
[34] S. Svelle, M. Visur, U. Olsbye, S. Saepurahman, M. Bjørgen, *Top. Catal.* **2011**, *54*, 897 – 906.
[35] T. Maihom, B. Boekfa, J. Sirijaraensre, T. Nanok, M. Probst, J. Limtrakul, *J. Phys. Chem. C* **2009**, *113*, 6654 – 6662.
[36] S. Saepurahman, M. Visur, U. Olsbye, M. Bjorgen, S. Svelle, *Top. Catal.* **2011**, *54*, 1293 – 1301.
[37] S. Svelle, M. Bjørgen, *J. Phys. Chem. A* **2010**, *114*, 12548 – 12554.
[38] D. Lesthaeghe, A. Horre, M. Waroquier, G. B. Marin, V. Van Speybroeck, *Chem. Eur. J.* **2009**, *15*, 10803 – 10808.
[39] D. M. McCann, D. Lesthaeghe, P. W. Kletnieks, D. R. Guenther, M. J. Hayman, V. Van Speybroeck, M. Waroquier, J. F. Haw, *Angew. Chem.* **2008**, *120*, 5257 – 5260; *Angew. Chem. Int. Ed.* **2008**, *47*, 5179 – 5182.
[40] K. Hemelsoet, A. Nollet, M. Vandichel, D. Lesthaeghe, V. Van Speybroeck, M. Waroquier, *ChemCatChem* **2009**, *1*, 373 – 378.
[41] K. Hemelsoet, A. Nollet, V. Van Speybroeck, M. Waroquier, *Chem. Eur. J.* **2011**, *17*, 9083 – 9093.
[42] D. Lesthaeghe, B. De Sterck, V. Van Speybroeck, G. B. Marin, M. Waroquier, *Angew. Chem.* **2007**, *119*, 1333 – 1336; *Angew. Chem. Int. Ed.* **2007**, *46*, 1311 – 1314.
[43] D. Lesthaeghe, J. Van der Mynsbrugge, M. Vandichel, M. Waroquier, V. Van Speybroeck, *ChemCatChem* **2011**, *3*, 208 – 212.
[44] M. Bjorgen, S. Akyalcin, U. Olsbye, S. Benard, S. Kolboe, S. Svelle, *J. Catal.* **2010**, *275*, 170 – 180.
[45] C. M. Wang, Y. D. Wang, Z. K. Xie, Z. P. Liu, *J. Phys. Chem. C* **2009**, *113*, 4584 – 4591.
[46] C. M. Wang, Y. D. Wang, H. X. Lie, Z. K. Xie, Z. P. Liu, *J. Catal.* **2010**, *271*, 386 – 391.
[47] J. Q. Chen, A. Bozzano, B. Glover, T. Fuglerud, S. Kvisle, *Catal. Today* **2005**, *106*, 103 – 107.
[48] F. Bleken, M. Bjorgen, L. Palumbo, S. Bordiga, S. Svelle, K. P. Lillerud, U. Olsbye, *Top. Catal.* **2009**, *52*, 218 – 228.
[49] B. V. Vora, T. L. Marker, P. T. Barger, H. R. Nilsen, S. Kvisle, T. Fuglerud in *Natural Gas Conversion Iv, Vol. 107*, Elsevier, Amsterdam, **1997**, 87 – 98.
[50] J. Liang, H. Y. Li, S. Zhao, W. G. Guo, R. H. Wang, M. L. Ying, *Appl. Catal.* **1990**, *64*, 31 – 40.
[51] H. Koempel, W. Liebnerin, *Natural Gas Conversion Viii, Proceedings of the 8th Natural Gas Conversion Symposium, Vol. 167* (Eds.: F. B. Noronha, M. Schmal, E. F. SousaAguiar), Elsevier, Amsterdam, **2007**, pp. 261 – 267.
[52] D. M. Marcus, W. G. Song, L. L. Ng, J. F. Haw, *Langmuir* **2002**, *18*, 8386 – 8391.
[53] B. P. C. Hereijgers, F. Bleken, M. H. Nilsen, S. Svelle, K. P. Lillerud, M. Bjorgen, B. M. Weckhuysen, U. Olsbye, *J. Catal.* **2009**, *264*, 77 – 87.
[54] S. Bordiga, L. Regli, C. Lamberti, A. Zecchina, M. Bjorgen, K. P. Lillerud, *J. Phys. Chem. B* **2005**, *109*, 7724 – 7732.
[55] W. Wang, Y. J. Jiang, M. Hunger, *Catal. Today* **2006**, *113*, 102 – 114.
[56] J. Z. Li, Y. X. Wei, J. R. Chen, P. Tian, X. Su, S. T. Xu, Y. Qi, Q. Y. Wang, Y. Zhou, Y. L. He, Z. M. Liu, *J. Am. Chem. Soc.* **2012**, *134*, 836 – 839.
[57] D. Lesthaeghe, V. Van Speybroeck, M. Waroquier, *Phys. Chem. Chem. Phys.* **2009**, *11*, 5222 – 5226.
[58] D. Lesthaeghe, V. Van Speybroeck, G. B. Marin, M. Waroquier, *J. Phys. Chem. B* **2005**, *109*, 7952 – 7960.
[59] E. Clar, M. Zander, *J. Chem. Soc.* **1957**, 4616 – 4616.
[60] *Catalytic Science Series, Vol. 3* (Eds.: P. Barger, M. Guisnet, J. P. Gilson), Imperial College Press, Danvers, **2002**, pp. 239 – 260.
[61] D. Chen, K. Moljord, T. Fuglerud, A. Holmen, *Microporous Mesoporous Mater.* **1999**, *29*, 191 – 203.
[62] I. M. Dahl, R. Wendelbo, A. Andersen, D. Akporiaye, H. Mostad, T. Fuglerud, *Microporous Mesoporous Mater.* **1999**, *29*, 159 – 171.
[63] S. Bordiga, L. Regli, D. Cocina, C. Lamberti, M. Bjorgen, K. P. Lillerud, *J. Phys. Chem. B* **2005**, *109*, 2779 – 2784.
[64] J. F. Haw, *Phys. Chem. Chem. Phys.* **2002**, *4*, 5431 – 5441.
[65] K. Hemelsoet, A. Ghysels, D. Mores, K. De Wispelaere, V. Van Speybroeck, B. M. Weckhuysen, M. Waroquier, *Catal. Today* **2011**, *177*, 12 – 24.
[66] L. Palumbo, F. Bonino, P. Beato, M. Bjorgen, A. Zecchina, S. Bordiga, *J. Phys. Chem. C* **2008**, *112*, 9710 – 9716.
[67] D. Lesthaeghe, G. Delcour, V. Van Speybroeck, G. B. Marin, M. Waroquier, *Microporous Mesoporous Mater.* **2006**, *96*, 350 – 356.
[68] D. Lesthaeghe, V. Van Speybroeck, G. B. Marin, M. Waroquier, *Chem. Phys. Lett.* **2006**, *417*, 309 – 315.
[69] S. A. Trygubenko, D. J. Wales, *J. Chem. Phys.* **2004**, *120*, 2082 – 2094.
[70] G. Henkelman, B. P. Uberuaga, H. Jonsson, *J. Chem. Phys.* **2000**, *113*, 9901 – 9904.
[71] T. Verstraelen, V. Van Speybroeck, M. Waroquier, *J. Chem. Inf. Model.* **2008**, *48*, 1530 – 1541.
[72] Gaussian 03, Revision E.01, M. J. Frisch, G. W. Trucks, H. B. Schlegel, G. E. Scuseria, M. A. Robb, J. R. Cheeseman, J. A. Montgomery, Jr., T. Vreven, K. N. Kudin, J. C. Burant, J. M. Millam, S. S. Iyengar, J. Tomasi, V. Barone, B. Mennucci, M. Cossi, G. Scalmani, N. Rega, G. A. Petersson, H. Nakatsu-

ji, M. Hada, M. Ehara, K. Toyota, R. Fukuda, J. Hasegawa, M. Ishida, T. Nakajima, Y. Honda, O. Kitao, H. Nakai, M. Klene, X. Li, J. E. Knox, H. P. Hratchian, J. B. Cross, V. Bakken, C. Adamo, J. Jaramillo, R. Gomperts, R. E. Stratmann, O. Yazyev, A. J. Austin, R. Cammi, C. Pomelli, J. W. Ochterski, P. Y. Ayala, K. Morokuma, G. A. Voth, P. Salvador, J. J. Dannenberg, V. G. Zakrzewski, S. Dapprich, A. D. Daniels, M. C. Strain, O. Farkas, D. K. Malick, A. D. Rabuck, K. Raghavachari, J. B. Foresman, J. V. Ortiz, Q. Cui, A. G. Baboul, S. Clifford, J. Cioslowski, B. B. Stefanov, G. Liu, A. Liashenko, P. Piskorz, I. Komaromi, R. L. Martin, D. J. Fox, T. Keith, M. A. Al-Laham, C. Y. Peng, A. Nanayakkara, M. Challacombe, P. M. W. Gill, B. Johnson, W. Chen, M. W. Wong, C. Gonzalez, J. A. Pople, Gaussian, Inc., Wallingford CT, **2004**.

[73] B. Chan, L. Radom, *J. Am. Chem. Soc.* **2006**, *128*, 5322 – 5323.

[74] B. Chan, L. Radom, *Can. J. Chem.* **2010**, *88*, 866 – 876.

[75] Y. Zhao, D. G. Truhlar, *J. Phys. Chem. C* **2008**, *112*, 6860 – 6868.

[76] A. Ghysels, D. Van Neck, V. Van Speybroeck, T. Verstraelen, M. Waroquier, *J. Chem. Phys.* **2007**, *126*, 224102.

[77] A. Ghysels, V. Van Speybroeck, T. Verstraelen, D. Van Neck, M. Waroquier, *J. Chem. Theory Comput.* **2008**, *4*, 614 – 625.

[78] S. Grimme, J. Antony, T. Schwabe, C. Muck-Lichtenfeld, *Org. Biomol. Chem.* **2007**, *5*, 741 – 758.

[79] G. C. Bond, M. A. Keane, H. Kral, J. A. Lercher, *Catal. Rev. Sci. Eng.* **2000**, *42*, 323 – 383.

[80] A. Ghysels, T. Verstraelen, K. Hemelsoet, M. Waroquier, V. Van Speybroeck, *J. Chem. Inf. Model.* **2010**, *50*, 1736 – 1750.

[81] E. Runge, E. K. U. Gross, *Phys. Rev. Lett.* **1984**, *52*, 997 – 1000.

[82] M. Petersilka, U. J. Gossmann, E. K. U. Gross, *Phys. Rev. Lett.* **1996**, *76*, 1212 – 1215.

[83] A. Dreuw, M. Head-Gordon, *Chem. Rev.* **2005**, *105*, 4009 – 4037.

[84] C. Jamorski, M. E. Casida, D. R. Salahub, *J. Chem. Phys.* **1996**, *104*, 5134 – 5147.

[85] A. Gorling, H. H. Heinze, S. P. Ruzankin, M. Staufer, N. Rosch, *J. Chem. Phys.* **1999**, *110*, 2785 – 2799.

[86] E. A. Eilertsen, M. H. Nilsen, R. Wendelbo, U. Olsbye, K. P. Lillerud, *Stud. Surf. Sci. Catal.* **2008**, *174*, 265 – 268.

[87] L. Karwacki, E. Stavitski, M. H. F. Kox, J. Kornatowski, B. M. Weckhuysen, *Angew. Chem.* **2007**, *119*, 7366 – 7369; *Angew. Chem. Int. Ed.* **2007**, *46*, 7228 – 7231.

[88] L. Karwacki, M. H. F. Kox, D. A. Matthijs de Winter, M. R. Drury, J. D. Meeldijk, E. Stavitski, W. Schmidt, M. Mertens, P. Cubillas, N. John, A. Chan, N. Kahn, S. R. Bare, M. Anderson, J. Kornatowski, B. M. Weckhuysen, *Nat. Mater.* **2009**, *8*, 959 – 965.

[89] L. R. Aramburo, E. de Smit, B. Arstad, M. M. van Schooneveld, L. Sommer, A. Juhin, T. Yokosawa, H. W. Zandbergen, U. Olsbye, F. M. F. de Groot, B. M. Weckhuysen, *Angew. Chem.* **2012**, *124*, 3676; *Angew. Chem. Int. Ed.* **2012**, *51*, 3616.

[90] L. R. Aramburo, L. Karwacki, P. Cubillas, S. Asahina, D. A. M. de Sinter, M. R. Drury, I. L. C. Buurmans, E. Stavitski, D. Mores, M. Daturi, P. Bazin, P. Dumas, F. Thibault-Starzyk, J. A. Post, M. W. Andeson, O. Terasaki, B. M. Weckhuysen, *Chem. Eur. J.* **2011**, *17*, 13773.

[91] K. Barbera, F. Bonino, S. Bordiga, T. V. W. Janssens, P. Beato, *J. Catal.* **2011**, *280*, 196 – 205.

[92] P. Sazama, B. Wichterlova, J. Dedecek, Z. Tvaruzkova, Z. Muilova, L. Palumbo, S. Sklenak, O. Gonsiorova, *Microporous Mesoporous Mater.* **2011**, *143*, 87 – 96.

[93] S. Svelle, L. E. Sommer, K. Barbera, P. N. R. Vennestrøm, U. Olsbye, K. P. Lillerud, S. Bordiga, Y. H. Pan, P. Beato, *Catal. Today* **2011**, *168*, 38 – 47.

Received: August 24, 2012
Published online on November 30, 2012